



Bamboo charcoal fused with polyurethane foam for efficiently removing organic solvents from wastewater: experimental and simulation

Zeyu Wang¹ · Liyong Hu² · Min Zhao² · Luyao Dai² · Dzmitry Hrynsphan³ · Savitskaya Tatsiana³ · Jun Chen¹

Received: 19 January 2022 / Accepted: 7 May 2022
© The Author(s) 2022

Abstract

The development of a multifunctional oil adsorbing material which could effectively and quickly separate oily wastewater is one of the focuses in water environment restoration. In this study, bamboo charcoal (BC) was used as an improver to modify polyurethane (PU) foam. The results of scanning electron microscope (SEM) and Fourier-transform infrared spectroscopy (FTIR) revealed that the addition of BC could effectively improve the mechanical properties of PU. The adsorption data exhibited that the BC-loaded PU (BC/PU) foam composites effectively removed seven organic solvents (OSs, including octane, petroleum ether, soybean oil, chlorobenzene, 1,2-dichloroethane, *n*-hexane, cyclohexane), and the maximum adsorption capacity of BC/PU was 23.6 g g⁻¹ when BC content was 5%. The order of pseudo-second-order kinetic constants and maximum adsorption capacity of seven OSs was octane < petroleum ether < soybean oil < chlorobenzene < 1, 2-dichloroethane < cyclohexane < *n*-hexane. Based on the experimental data and density functional theory (DFT) simulation, the adsorption mechanism of OSs on BC/PU-5 was discussed. The E_{HOMO} and μ of OSs calculated by DFT were highly correlated with absorption affinity (K_2 , Q_e and Q_{max}). Hence, the contribution of OSs to the adsorption efficiency of BC/PU-5 may be mainly due to electron donor–acceptor (EDA) interaction and non-hydrophobic interaction. In addition, the adsorption capacity did not change significantly after repeated recycling 5 times. Overall, the prepared BC/PU foam composites could be used as a potential candidate for separating OSs in engineering applications.

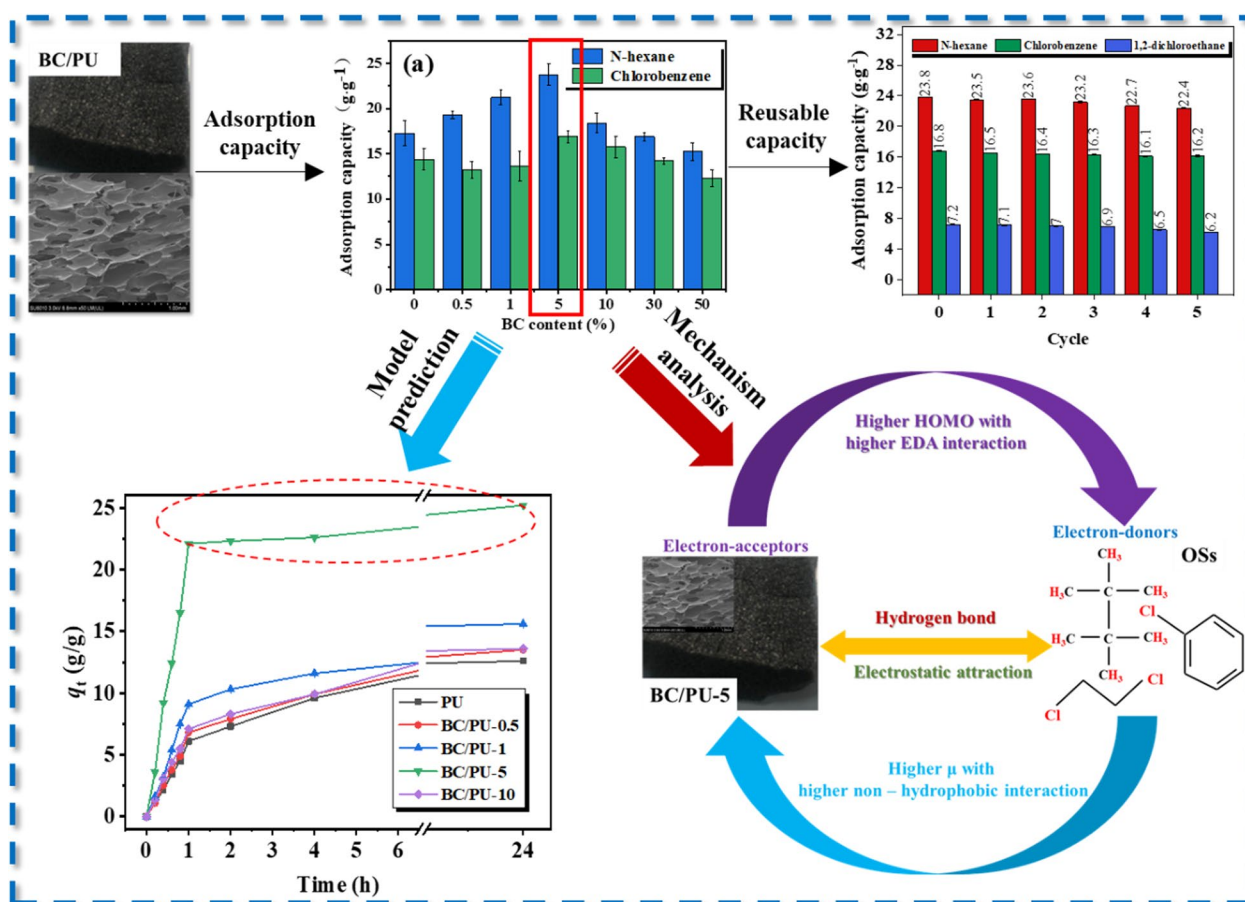
✉ Jun Chen
bec@zjut.edu.cn

¹ Key Laboratory of Pollution Exposure and Health Intervention of Zhejiang Province, Interdisciplinary Research Academy, Zhejiang Shuren University, 310015 Hangzhou, People's Republic of China

² College of Environment, Zhejiang University of Technology, Hangzhou 310032, People's Republic of China

³ Research Institute of Physical and Chemical Problems, Belarusian State University, 220030 Minsk, Belarus

Graphical Abstract



Highlights

1. The adsorption performance of BC/PU-5 for n-hexane reached the maximum of 23.6 g g⁻¹.
2. Based on the kinetic calculation and DFT simulation, the adsorption mechanism of OSs on BC/PU-5 was discussed.
3. The quantitative correlation between the structural parameters of OSs and the adsorption properties of BC/PU-5 was established.

Keywords Bamboo charcoal · Polyurethane · Adsorption · Organic solvent · Reusability

1 Introduction

With the leakage of organic solvents (OSs) in the process of transportation, offshore oil exploitation and industrial oily wastewater discharge, the aquatic environment has been

seriously damaged (Li et al. 2019a; Simha et al. 2018). At present, a variety of methods have been used to separate OSs from water, including adsorption (Benally et al. 2019; Brusseau 2019; Meng et al. 2019), flocculation (Vandamme et al. 2018), membrane separation (Zhao and Chung 2018), solvent extraction (Chang 2020), biodegradation (Tandjaoui et al. 2019; Wang et al. 2018a, b), in-situ combustion (Xiang et al. 2018) and solidification (Jia et al. 2019). The adsorption method is given priority due to its low cost, easy operation and fast response, which is widely regarded as an effective choice for treating OSs-bearing wastewater (Benally et al. 2019; Li et al. 2019b; Wu et al. 2017). Moreover, the traditional adsorption materials, such as activated carbon (Piail et al. 2019), sugar cane bagasse (Tahir et al. 2016), vegetable fibers (Xu et al. 2019), sawdust bed (Gao et al. 2018; Khasri and Ahmad 2018), vermiculite (Akemoto et al. 2021; Moraes et al. 2019), etc. have been put in practical use already. All of them have the disadvantages such as low adsorption efficiency, poor selectivity and unable to recycle.

Therefore, the preparation of a new type of adsorption material with high selectivity, large adsorption capacity, fast efficiency, excellent recyclability, and low cost has potential significance for oil–water separation (Brusseau 2019).

Polyurethane (PU) sponge is a good choice for its industrial application as an adsorbent due to its low cost, mass production, low specific gravity, good adsorption capacity and high specific surface area. However, the surface of unmodified PU is highly hydrophilic, which is not conducive to oil–water separation. The wettability of the adsorbent determines the wetting phenomenon and plays a crucial role in the oil–water separation process. The selective adsorption of oil by changing its wetting properties through surface modification of PU is one of the current research hotspots.

Numerous methods have been reported for surface modification of PU to convert the super-hydrophilic surface of PU into a superhydrophobic/oleophilic surface. Lundin et al. (2017) reported that graphene-modified PU and nano-kaolin-modified PU exhibited super-hydrophobicity with water contact angles of 152.3° and 156.5°, respectively. Maddalena et al. (2018) used graphene to modify the PU surface and reported the transformation of the super-hydrophilic surface of PU to a superhydrophobic/oleophilic surface. However, the development and application of graphene in oil–water separation is still limited by the following challenges, including high cost and biotoxicity. Therefore, it is of great significance to develop an environmentally friendly and low-cost material for PU modification and oil–water separation.

Because bamboo charcoal (BC) powder has the advantages of large specific surface area, high hydrophobicity, rich surface groups and low cost, it was selected to be loaded into PU in this study. The main objectives were as follows: (1) The effect of BC on the hydrophobicity, thermal stability and mechanical properties of PU was discussed; (2) The structural parameters of BC/PU were calculated by density functional theory (DFT); (3) The relationship between the molecular structure parameters and adsorption affinity of OSs was established; (4) The possible adsorption mechanisms was proposed.

2 Materials and methods

2.1 Materials

Polyether polyol (NJ-300, $M = 3000 \text{ g}\cdot\text{mol}^{-1}$), toluene diisocyanate (TDI, purity $\geq 99.0\%$ and $-\text{NCO}$ content $\geq 35.0\%$) were supplied by Runhong Chemical Co., Ltd in Jiangsu, China. BC powder was obtained from Lvyi Bamboo Charcoal Co., Ltd in Zhejiang, China. Dibutyltin dilaurate, triethylene diamine (as catalyst), silicone oil ($[-\text{Si}(\text{CH}_3)_2\text{O}-]_n$) (as a foam stabilizer), and sterile water (as a blowing agent) were purchased from Aladdin, China. All chemicals and

solutions were of analytical grade or chromatographically pure.

2.2 Preparation of BC/PU foam composites

BC was grounded into powder, and passed through 8000 mesh sieves. Then it was washed with sterile water and $0.1 \text{ mol}\cdot\text{L}^{-1}$ phosphate for 3–5 times to remove the dusting.

The BC/PU foam composites were synthesized by a one-step method (Fig. S1). The details were as follows: a certain amount of NJ-330, coal, silicone oil, sterile water, dibutyltin dilaurate, and triethylene diamine were premixed in a plastic cup, and stirred at a speed of about 1000 rpm for 5–10 min to obtain a polyol mixture. TDI was added to the polyol mixture and stirred at the same speed for 10–20 s until the mixture foamed. Then the mixture was immediately transferred to the oven and baked at $100 \text{ }^\circ\text{C}$ for 2 h. Based on different content of BC (0, 0.5, 1, 5, 10, 30, 50 wt%), a series of BC/PU materials were prepared and named as BC/PU-0, BC/PU-0.5, BC/PU-1, BC/PU-5, BC/PU-10, BC/PU-30, BC/PU-50, respectively. The BC/PU sample drawing was shown in Fig. S1. The basic recipe of BC/PU foam composites was shown in Table S1.

2.3 Sample characterization

A scanning electron microscope (SEM; Gemini 300, Germany) was used to examine the state of the BC and BC/PU foam. Thermogravimetric analysis (TGA) was carried out by an instrument (STA 449 C), under N_2 atmosphere at a heating rate of $10 \text{ }^\circ\text{C}\cdot\text{min}^{-1}$. The functional groups and chemical structures were confirmed using a Nicolet FT-IR spectrometer via potassium bromide (KBr) pellet. Three measurements at different portions of one sample were collected over the range of $4000\text{--}600 \text{ cm}^{-1}$ at 4 cm^{-1} and 16 co-added scans. The water contact angles of BC and BC/PU foam were test by the sessile drop method. The droplet volume used in the experiment was about $4 \text{ }\mu\text{L}$ and 5 different points on the same sample surface were taken to measure the contact angle. The mechanical properties of standard shape samples were tested using an Instron universal testing machine (model 4502) with a crosshead speed of 40 mm min^{-1} (Mikusova et al. 2020). The samples were put into the self-made mold for foaming and then taken out. After ripening, the slurry was cut into dumbbell shaped samples as shown in Fig. S3. The average value of 5 samples was measured.

2.4 Oil adsorption

In order to investigate the adsorption performance of the BC/PU foam composites, they were cut into the same size, immersed in a sufficient amount of OSs, and weighed at

room temperature. The adsorption properties of BC/PU foam composites were calculated according to the following Eq. (1):

$$Q(\text{g g}^{-1}) = \frac{(m_t - m_0)}{m_0} \quad (1)$$

where m_t and m_0 are the weight of the OSs adsorbents dispersed in oil for time t and the dry weight of the OSs adsorbent, respectively.

The BC/PU foam composites were immersed in HCl and NaOH ($1 \text{ mol}\cdot\text{L}^{-1}$) solvents, dried and weighed to evaluate their durability after 24 h. Equation (2) is as follows:

$$W_m = \frac{(C_1 - C_0)}{C_1} \times 100\% \quad (2)$$

where W_m is the durability (%), C_1 is the initial quality of the sample, C_0 is the final quality of the sample.

All experiments were carried out in triplicate, and the data shown in the corresponding figures were the mean values of the experimental results.

2.5 Oil adsorption kinetics

The BC/PU foam composites were cut into about 10 mm squares, weighed and immersed in oil. They were weighed again after 48 h of maximum contact time. The maximum adsorption capacity was determined by Eq. (3):

$$A = \frac{m_s - m_e}{m_e} \quad (3)$$

where A is the oil adsorption capacity (g g^{-1}); m_s is the mass of BC/PU foam composites saturated with oil (g); and m_e is the mass of the BC/PU (g) with no oil adsorbed.

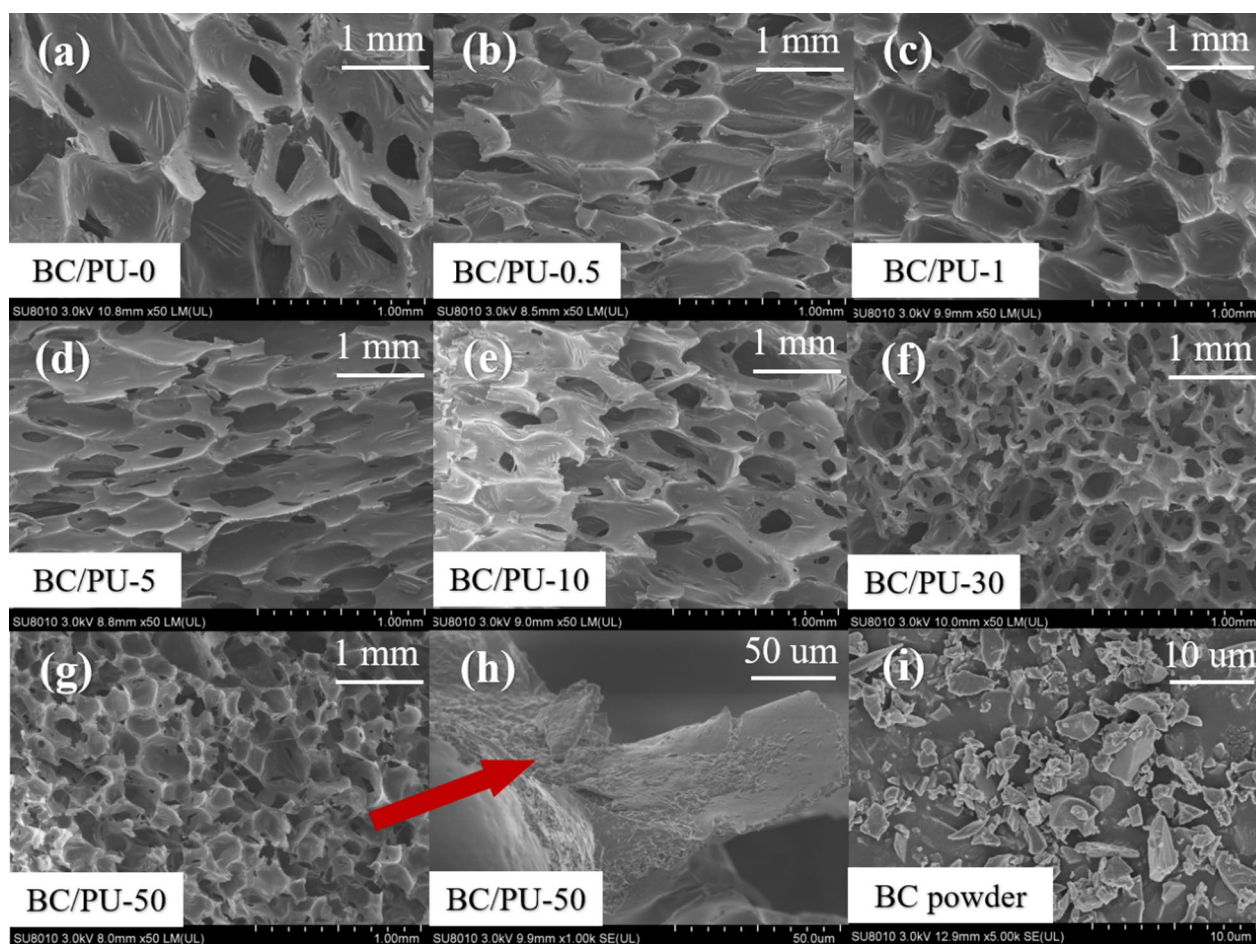


Fig. 1 SEM images of BC/PU-0 (a), BC/PU-0.5 (b), BC/PU-1 (c), BC/PU-5 (d), BC/PU-10 (e), BC/PU-30 (f), BC/PU-50 (g), BC/PU-50 (h, $\times 1000$) and BC powder (i)

2.6 Oil adsorption isotherms

Studying the adsorption behavior by adsorption isotherms could indicate the way of oil adsorption and estimate the maximum amount of BC/PU foam composites. The adsorption behavior of different oil concentrations (10 to 200 g L⁻¹) was investigated at room temperature with BC/PU-5 foam composites. The Langmuir and Freundlich isotherm models were analyzed to determine the adsorption behavior of the BC/PU-5 foam composites. Please refer to the Supplementary Materials for experimental conditions and steps in detail.

2.7 DFT calculation methods

All density functional theory (DFT) calculations in this study were performed using the DMol³ package in Materials Studio, which utilizes the first-principles method in Generalized Gradient Approximation (·A) and the Perdew–Burke–Ernzerhof (PBE) function. The adsorption energy of OSs molecules on the surface is calculated by the following formula:

$$E_{ads} = E_{surface+OSs} - (E_{surface} + E_{OSs}) \quad (4)$$

where $E_{surface}$ and E_{OSs} represent the energy of substrate surface and free OSs molecules respectively, and $E_{surface + OSs}$ is the total energy of adsorbate surface complex. A negative value of E_{ads} indicates that the process is exothermic. The greater the absolute value of E_{ads} , the stronger the corresponding interaction. A positive value indicates that adsorption does not occur. Details of the calculation parameters and adsorption model structure are described in the Supplementary Material.

2.8 Recycling of the adsorbent

To test the regeneration properties of the BC/PU foam composites, the adsorbed oils and OSs were observed from the foam by compression. Then, the oils adsorbed BC/PU foam composites were immersed in sufficient amount of anhydrous ethanol for desorption and dried at 100 °C for 24 h. The oil adsorption and desorption process of the BC/PU foam composites was repeated 5 times to determine their reusability. For each cycle, the BC/PU foam composites were weighed before and after oils or OSs adsorption.

3 Results and discussion

3.1 Characterization of BC/PU foam composites

The SEM results of PU with different additions of BC powder were illustrated in Fig. 1. With the increase of BC

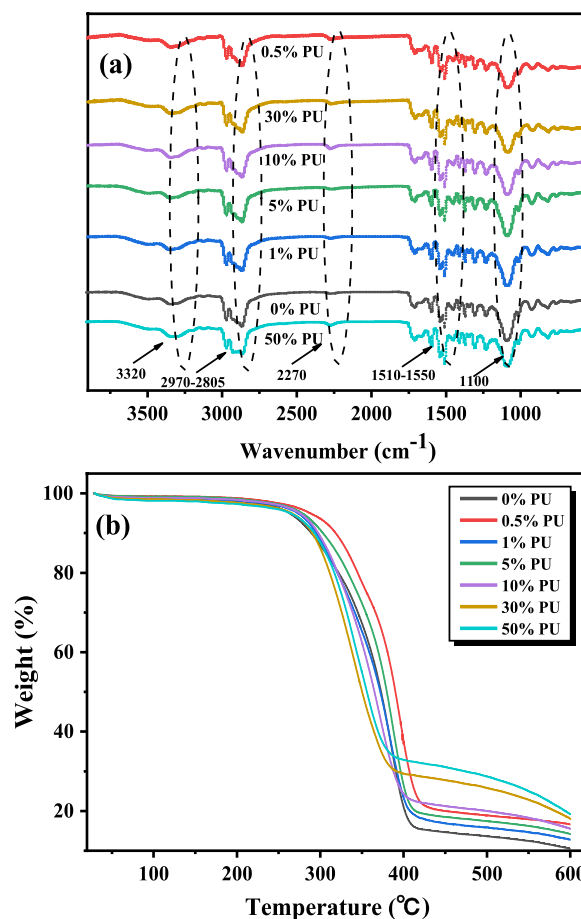


Fig. 2 The FT-IR and TGA curves of the BC/PU foam composites

powder, the number of pores increased significantly, yet there were also different degrees of closed-cell phenomenon. This was because the BC powder acting as an additional particle that could promote the heterogeneous nucleation of CO₂ generated during the synthesis. When the bubble film of the PU was thick, the bubble punching was not finished brewing or crushing. As showed in Fig. 1h, the surface of the PU skeleton was smooth, indicating that the BC powder was wrapped well as the filling material, and basically would not overflow. It could be proved that BC was well filled into the PU framework structure (After cleaning and drying, put in the aqueous solution, the solution did not turn black).

The FT-IR spectra of BC/PU foam composites were shown in Fig. 2a. The existence of O–H, C–H, C=O, C=C and many single bond extensions could be observed. Since pure PU has only three main elements (C, H and O), a limited number of bond vibrations could be assigned to the peaks in FTIR. PU is a hydroxyl rich polymer, which causes some hydroxides and possible water to remain in the sample after pyrolysis. Therefore, the peak at 3320 cm⁻¹ could be attributed to OH stretching (Wang et al. 2021). Aliphatic C–H stretching was observed at 2970 cm⁻¹, which confirmed

that PU was not completely carbonized during pyrolysis. A wide asymmetric peak with a maximum at 2270 cm^{-1} was caused by C–O stretching. The peak contains a variety of C=O containing functional groups, including ketones, carboxylic esters and anhydrides. The band at 1550 cm^{-1} could be attributed to C=C bond stretching from aromatic rings in PU and new aromatized and carbonized materials from dehydration and cyclization of carbohydrate rings during pyrolysis (Wang et al. 2020). The expected peaks of single bond stretching and other deformation bands at 1100 cm^{-1} were also observed. These are numerous and overlapping, and are difficult to allocate in the average spectrum.

With the increasing of BC powder content, the number of peak shapes did not change, indicating that BC powder was well dispersed and did not react with the matrix during the synthesis of PU. As showed in Fig. 2a, compared with pure PU, the prepared BC modified PU foam had stronger N–H bond tensile vibration at 3220 cm^{-1} and C–H tensile vibration at 2973 cm^{-1} . Moreover, with the increase of BC content, the adsorption peaks of BC/PU were broader and enhanced from 1600 to 500 cm^{-1} . The little –NCO adsorption peak at 2270 cm^{-1} was observed, which means that the reaction was guaranteed to complete.

Figure 2b and Table 1 show the thermogravimetric (TGA) curves and data of BC/PU foam composites. When the temperature was $600\text{ }^{\circ}\text{C}$, the maximum weight loss rate of pure PU could reach 89.508% , and when the addition amount of BC powder was 50% , the weight loss rate was only 80.813% . The results revealed that as the content of BC powder increased, the thermal stability of PU also increased. These results could be due to the fact the BC particles had the effect of heat dissipation on the PU, which increased the thermal decomposition temperature and reduced the mass of heat loss (Pan et al. 2020). It was also possible that the BC powder was carbonized and fired at high temperature, and had high temperature resistance itself. During the synthesis process, it became the skeleton of PU, thus improving the thermal stability of BC/PU foam composites (Kuo et al. 2012).

Table 1 The thermal weightlessness of BC/PU foam composites

PU	T_5 ($^{\circ}\text{C}$)	T_{10} ($^{\circ}\text{C}$)	T_{max} ($^{\circ}\text{C}$)	Weight loss ratio (%)
BC/PU-0	262.86	289.34	363.73	89.508
BC/PU-0.5	267.34	290.31	362.52	87.934
BC/PU-1	271.51	292.14	361.15	86.198
BC/PU-5	275.97	303.96	355.62	85.371
BC/PU-10	278.34	302.07	353.01	84.503
BC/PU-30	279.05	301.12	345.63	82.121
BC/PU-50	263.71	292.07	342.89	80.815

The wettability of BC/PU foam composites was one of the most important considerations when choosing a suitable OSs adsorbent. The hydrophobic property of PU foam was determined by measuring the Water Contact Angle (WCA) between the sample surface and water (polar liquid) (Luo et al. 2018; Meng et al. 2018). With the incorporation of BC powder, the hydrophobicity of PU changed remarkably. As shown in Fig. 3, the hydrophobicity of BC/PU foam composites was good and the maximum WCA of BC/PU-5 was 137.2° , which proved that the introduction of BC could effectively improve the hydrophobicity of PU foam. Therefore, a higher WCA could enhance the selectivity and interaction between PU foams and OSs, leading to higher adsorption efficiency in heterogeneous OSs-water systems. Guselnikova et al (2020) reported a modified PU with superhydrophobic properties provided by Fe and acetonitrile with a WCA value of $168 \pm 1^{\circ}$, but this does not seem to be the best choice considering the environmental friendliness.

3.2 Mechanical property of BC/PU foam composites

In practical engineering application, the mechanical properties of materials are the main basis for determining the design parameters of operation (Zhang et al. 2018). Other studies have illustrated that the type, aperture size, surface modification and interaction with PU of the filler have the greatest influence on the mechanical performance of the obtained materials (Lu et al. 2021). Therefore, the tensile properties, elastic modulus and elongation at break of BC/PU foam composites in this study were tested.

Table S2 shows the effect of different loading levels of BC on different mechanical properties of PU, namely tensile strength, elastic modulus and elongation at break. Pinto et al. (2015) have reported that the addition of BC powder could improve the tensile strength of PU. The tensile strength of BC/PU foam composites depended on many factors, such as crosslink density and polymer-filler interactions. The tensile strength was positively correlated with crosslinking density and polymer filler interaction. The increase of PU tensile strength after adding BC was attributed to the increase of crosslinking density. SEM images have confirmed the good dispersion of BC in PU matrix (Fig. 1). With the increase of BC content in the composites, the tensile strength first increased gradually and then decreased. Compared with 0.05 MPa of pure PU, the tensile strengths of BC/PU composites were 0.13 MPa , 0.16 MPa , 0.21 MPa , 0.12 MPa , 0.05 MPa , 0.02 MPa at BC loading rates of 0.5% , 1% , 5% , 10% , 30% , and 50% , respectively. This was due to the poor dispersibility of BC at high concentrations. At higher BC crosslinking densities, the polymer matrix stiffened and the crosslinks between polymer chains retarded segmental motion, leading to sample fracture at lower elongations. This

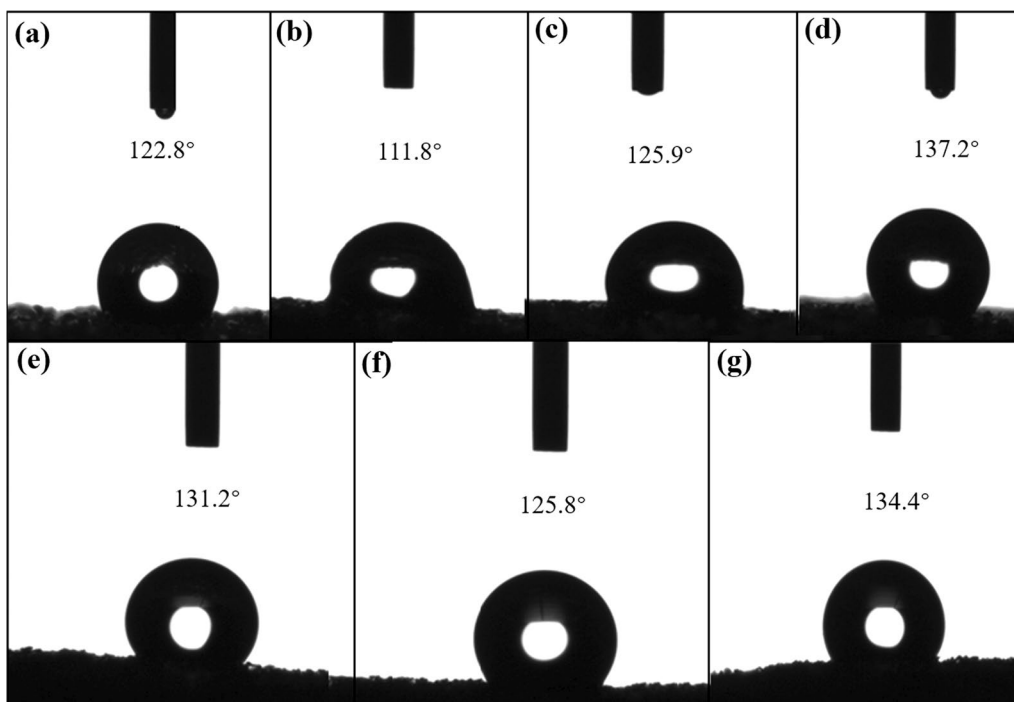


Fig. 3 The WCA of BC/PU foam composites

could be verified from the changing trend of elongation at break.

The modulus of elasticity of a composite was often used as an indicator of its stiffness. The higher the stiffness, the higher the elastic modulus of the composite material. It could be seen from Table S2 that the elastic modulus and tensile properties showed the same trend, which may be because the BC powder acted to connect the macromolecules inside the PU when the foam was subjected to external force, thereby increasing the strength of the foam. However, when the BC content was too high, agglomeration would occur during the synthesis of PU, which would affect the gel reaction, resulting in the inability to find effective connections between polymers, and some hollow bottom droplets may appear, resulting in declining of mechanical properties (Singh et al. 2019). The results revealed that the mechanical properties of BC/PU foam were improved effectively after adding less BC powder, which provides an effective basis for the application in other fields.

Table 2 shows the influence of BC powder addition on the durability of PU foam. Compared with pure PU, the durability of PU foam was improved after adding BC powder, but the change pattern was not linear. BC/PU-5 had the best acid resistance, and BC/PU-10 had the best alkaline resistance. This may be due to the inertness of the BC powder. After the BC powder became a part of the PU skeleton, it was not easy to react with other compounds, thereby improving the durability of the BC/PU foam (Goo et al. 2019; Sato et al. 2018).

Table 2 The durability of BC/PU foam composites

Samples	Acid resistance (%)	Alkali resistance (%)
BC/PU-0	76.8	81.3
BC/PU-0.5	79.6	86.3
BC/PU-1	92.7	91.2
BC/PU-5	94.6	90.3
BC/PU-10	93.3	93.4
BC/PU-30	86.6	87.6
BC/PU-50	87.3	89.5

3.3 OSs adsorption behavior

In the foaming synthesis process, the content of modified materials played a key role and also determined the adsorption performance of the PU composites (Morita et al. 2017). The effect of BC content on the adsorption of OSs is showed in Fig. 4a. It could be clearly observed that the adsorption properties of BC/PU foam first increased and then decreased with the increasing of BC content, and the adsorption properties of PU composites reached the maximum when the BC content was 5%. The maximum adsorption capacities of n-hexane and chlorobenzene by BC/PU composite were 23.6 g g⁻¹ and 18.1 g g⁻¹, respectively. Obviously, this was

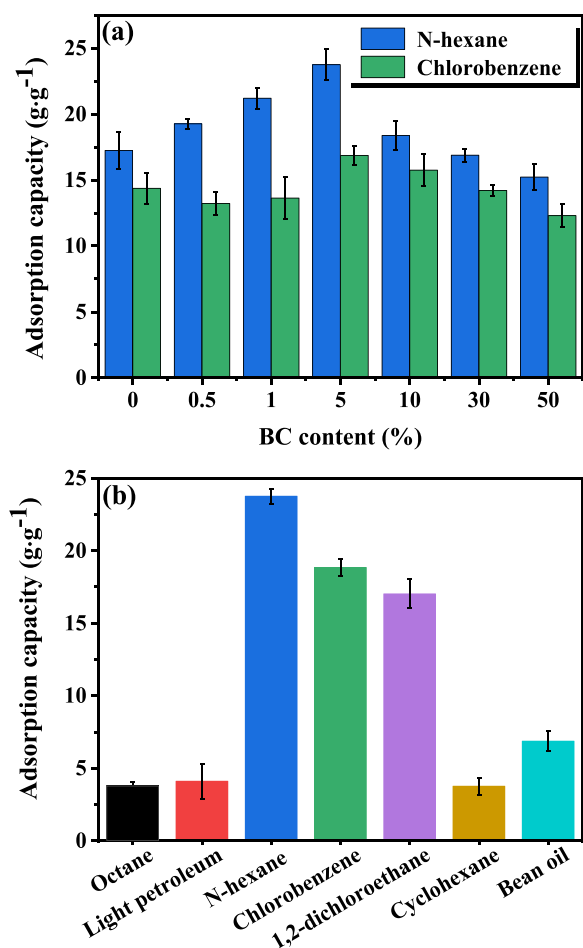


Fig. 4 Adsorption properties of BC/PU foam composites affected by the wt% of BC (a) and adsorption properties of the BC/PU-5 foam composites for OSs (b) (foam sample of 1 g, OSs concentration 100 mg·L⁻¹, 30 °C, and pH 7.0)

significantly superior to inorganic nanowire membranes. The results showed that the strong adsorption property of BC powder was well utilized in this system, so that the prepared PU foam had a good adsorption property, and BC/PU-5 showed the best adsorption performance. Therefore, BC/PU-5 was selected for the further study. Li et al. (2016) dispersed superhydrophobic/lipophilic apt of different quality into the cleaned PU sponge (0%, 10%, 15%, 20%, 25%, 30%, 35%, 40%) to obtain superhydrophobic adsorption material, and its maximum adsorption capacity for OSs was 17.1 g g⁻¹. Khosravi et al. (2015) synthesized a highly hydrophobic and lipophilic modified PU through simple vapor deposition, polypyrrole polymerization and palmitic acid modification, and its maximum adsorption capacity for OSs was 21.3 g g⁻¹. At the same time, the comparison of adsorption capacity of different PU materials was also listed (Table S9) in the Supplementary Materials. Compared with other materials, BC, as a modified material of PU, has greater adsorption capacity for OSs.

The BC/PU-5 foam composites were cut to the same size, immersed in sufficient amounts of octane, petroleum ether, soybean oil, chlorobenzene, 1, 2-dichloroethane, cyclohexane, and n-hexane, respectively. As shown in the Fig. 4b, BC/PU-5 foam composites had selective adsorption on these OSs, which may be due to the fact that the density and viscosity of the solvent itself had a significant impact on the adsorption efficiency (Chen et al. 2021). The results showed that BC/PU foam composites exhibited excellent adsorption properties for these OSs, among which the adsorption capacities of n-hexane, chlorobenzene and 1,2-dichloroethane were 23.6 g g⁻¹, 18.1 g g⁻¹ and 16.5 g g⁻¹, respectively. The OSs adsorption performance of the PU foams was closely related of the microporous structure and expansion propertied (Neimark and Grenev 2020). In addition, the density, viscosity and molecular weight of the PU as well as the physical and chemical properties of the OSs adsorbent had a great influence on the OSs adsorption performance.

In order to test the adsorption performance of the BC/PU-5 foam composites, n-hexane and chloroform were selected as representative OSs. For the convenience of observation, the red dye solution was used for dyeing. As shown in Fig. 5, n-hexane and chloroform were added to the water to form an insoluble mixture, and then a small piece of BC/PU-5 foam composite was placed on the surface of the mixture. It could be seen that the OSs in the water were quickly adsorbed, a clear and transparent water was obtained. This was because the OSs were rapidly adsorbed and stored in the abundant open cells and micropores of the BC/PU-5 foam composite after contacting with the BC/PU-5 foam composite, achieving the purpose of adsorption and separation. In addition, no OSs dripping was observed during the treatment. These results have revealed that the synthesized BC/PU-5 foam composites have strong adsorption performance and great potential in the treatment of OSs.

3.4 Kinetic study of OSs adsorption capacity with BC/PU-5 foam composites

n-Hexane was selected as the representative of OSs in wastewater. As shown in Fig. 6a, the time-dependent adsorption capacity (q_t) of BC/PU foam composites with different BC content to n-hexane was measured in an aqueous solution at room temperature and pH 7.0. For BC/PU foam composites, with the increasing of BC content, the final adsorption capacity of n-hexane increased, and BC/PU-5 has the highest adsorption capacity. On the other hand, based on the pseudo-second-order kinetic model, the adsorption kinetics of OSs on BC/PU foam composites were analyzed, which was expressed as follows:

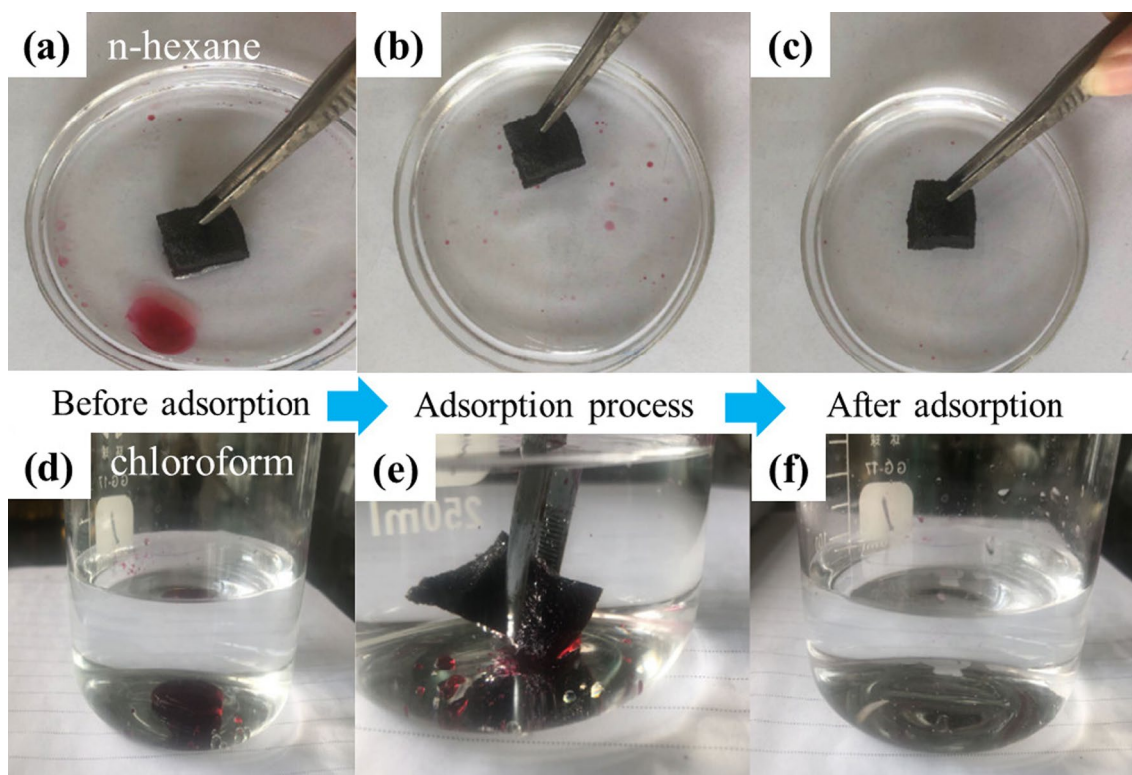


Fig. 5 Adsorptive performance of BC/PU-5 foam composites for n-hexane (a-c) and chloroform (d-f) (foam sample of 1 g, OSs concentration 100 mg·L⁻¹, 30 °C, and pH 7.0)

$$\frac{t}{q_t} = \frac{1}{kq_e^2} + \frac{t}{q_e} \tag{5}$$

Among them, *t* is the contact time between the adsorbate and the adsorbent (*h*), *q_t* and *q_e* are the adsorbate content removed by the adsorbent at any time *t* and equilibrium (g g⁻¹), and *k* is the rate constant g (g h)⁻¹. As shown in Fig. 6b, it was found that the adsorption kinetics of BC/PU foam composites prepared in this study were in accordance with the pseudo-second-order kinetic model. This indicated that the chemical adsorption between BC/PU foam composites and n-hexane may be the rate determining stage of the entire adsorption process (Wang et al. 2018a). The *q_{e, cal}* and *k* parameters were directly evaluated from the slope and intercept of the *t/q_t* vs. *t* curve, and summarized in Table 3. The calculated *q_{e, cal}* values were very consistent with the experimental *q_e*. The exp value was measured when the contact time was 24 h, and the value was directly proportional to the BC content in the BC/PU foam composites. It was also worth noting that as the BC content in the syntactic foam increased from 0.5% to 5%, the equilibrium rate constant *k* decreased from 0.318 to 0.219 g (g h)⁻¹.

It should be mentioned that the *q_t* values of all samples in Fig. 6a did not reach equilibrium within 24 h. Even in 24 h, the curve showed an increasing trend. However, the *q_{e, exp}* value (Table 3) was calculated from the slope of the linear graph by applying the *q_t* data in Fig. 6a to Eq. (5). As shown in Fig. 6b, the slope showed good linearity within 24 h, so it would not change even for a longer period time. This revealed that the *q_{e, cal}* values were almost the same as the *q_{e, exp}* value. Therefore, it was reasonable to believe that the 24 h *q_t* value was very close to the equilibrium value.

3.5 Effect of initial pH

Adsorption removal of various OSs by BC/PU foam composites at initial pH ranging from 1 to 11 was studied. As can be seen from Fig. 7a, the adsorption efficiency of OSs increased with the increasing of initial pH from 1 to 3, and gradually decreased when the initial pH was > 3. Therefore, when the initial pH was 3, the adsorption efficiency of OSs was the highest, and the adsorption efficiency could reach more than 80% (octane: 87.30%; light petroleum: 80.15%;

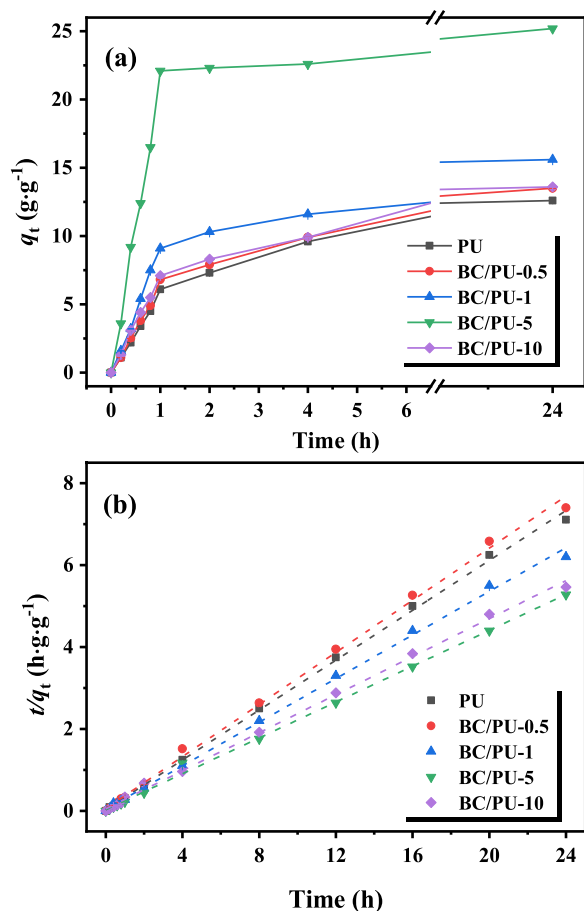


Fig. 6 Time-dependent OSs adsorption capacity (q_t) (a) and plots of t/q_t versus t based on the pseudo-second order kinetics (b) of BC/PU foam composites in aqueous solutions (foam sample of 0.1 g, n-hexane concentration of 0.01 wt%, 30 °C, and pH 7.0)

Table 3 Pseudo-second order kinetic parameters and experimental ultimate n-hexane adsorption capacities for BC/PU foam composites

Adsorbents	$q_{e,cal}$ (g g ⁻¹)	k g (g h) ⁻¹	R^2	$q_{e,exp}$ (g g ⁻¹)
PU	15.27	0.304	0.996	16.22
BC/PU-0.5	16.36	0.318	0.997	17.35
BC/PU-1	18.54	0.266	0.993	19.51
BC/PU-5	25.65	0.219	0.998	26.63
BC/PU-10	19.53	0.232	0.994	18.51

bean oil: 88.24%; chlorobenzene of 96.96%; 1,2-dichloroethane; 95.26% cyclohexane 87.12%; N-hexane 98.63%).

In order to further understand the influence of pH on the adsorption of OSs, the PZC of BC/PU was determined. As can be seen from Fig. 7c, the PZC value of BC/PU was about 2.5, hence BC/PU had a positive charge when pH was less than 2.5 and a negative charge when pH was greater than 2.5.

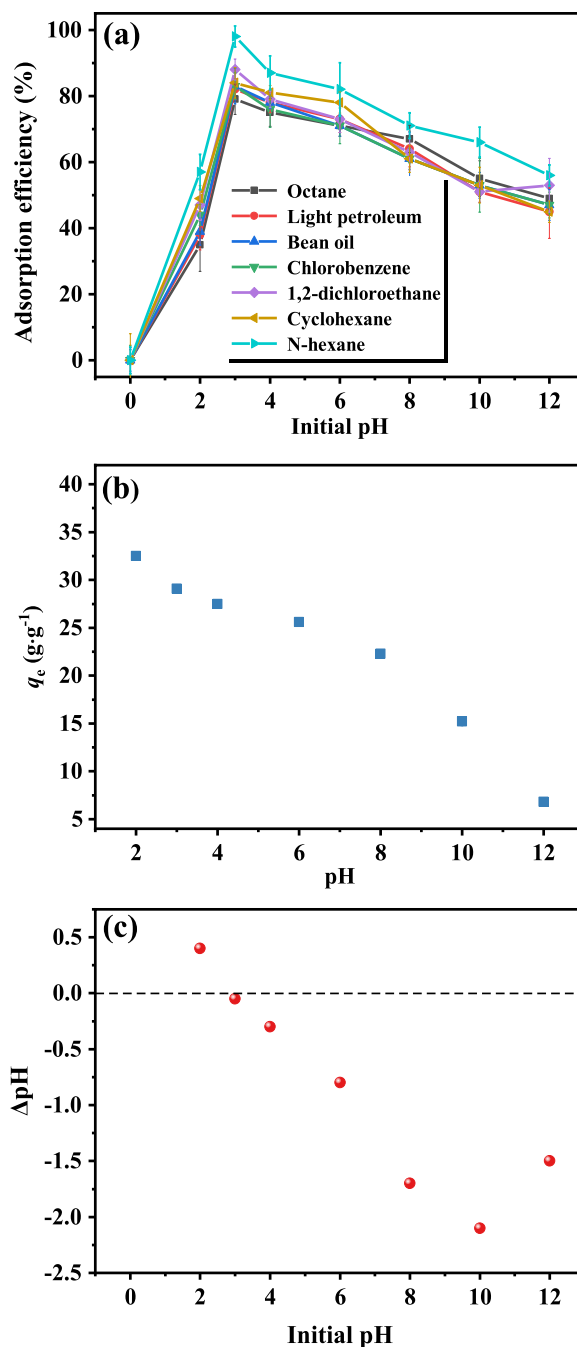


Fig. 7 Effect of initial pH on adsorption (a) and n-hexane adsorption capacities (q_e) of BC/PU-5 foam composites (b) (initial OSs concentration = 100 mg·L⁻¹, BC/PU-5 dosage = 1 g·L⁻¹, reaction temperature = 298 K, adsorption time = 2 h) and PZC analysis of BC/PU-5 (c)

On the other hand, most OSs have different morphologies (ionized or neutral) at different pH values, which are related to their ionization constant (pK_a). Various OSs were in slight transition of protonation-deprotonation at $pK_{a1} < 3 < pK_{a2}$ which might enhance the adsorption affinity. In addition, at low pH, various OSs could form hydrogen bonds through

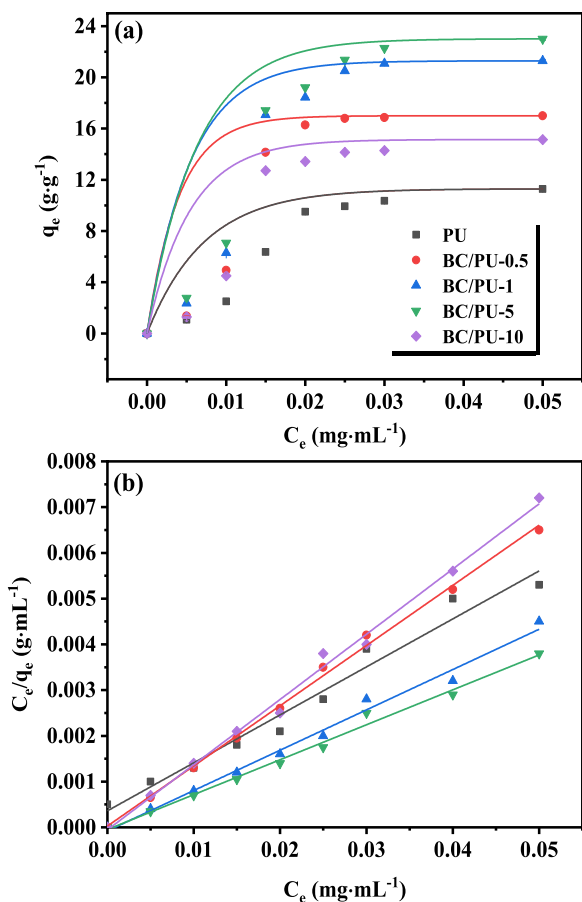


Fig. 8 Equilibrium *n*-hexane adsorption capacity (q_e) (a) and plots of C_e/q_e versus C_e base on Langmuir isotherm model (b) of BC/PU foam composites in aqueous solutions (foam sample of 0.1 g, 30°C, and pH 7.0)

electron donor–acceptor (EDA) interaction, which promoted the adsorption performance of OSs on BC/PU. When the pH was > 3, the types of anions were enriched with the increasing of pH value, which reduced the electrostatic attraction, resulting in a significant reduction in the adsorption efficiency of OSs. It was also confirmed by other scholars that *n*-hexane adsorption was most effective when the solution was adjusted to pH 3, which was consistent with this study (Alswieleh et al. 2021; Ghafari et al. 2019).

It was determined that the BC/PU-5 foam composites adsorbed about 32.7 g g⁻¹ of *n*-hexane with an initial pH of 2.0. The adsorption capacity of *n*-hexane decreased as the pH value increased. At lower pH values, the final *n*-hexane adsorption capacity of BC/PU-5 foam composites was higher, which may be due to the special interaction between the protonated amino groups of PU and the alkyl ions of *n*-hexane molecules. As described above, the amino groups in PU had a higher degree of protonation under acidic conditions, which ultimately led to a higher chemical adsorption of *n*-hexane by PU (Chen et al. 2020).

The above results revealed that BC/PU-5 has poor adsorption effect on OSs in alkaline solution. Therefore, OSs could be easily desorbed from depleted BC/PU using dilute alkaline solution. In this study, 0.1 M NaOH solution was employed to desorb OSs from the depleted sorbent, and it was shown that 95–99% of the OSs could be desorbed (data not shown).

3.6 Adsorption isotherms with BC/PU-5 foam composites

The adsorption isotherm described how the adsorbate interact with the adsorbent, which was essential for optimizing the use of the adsorbent. Therefore, the correlation between the experimental equilibrium isotherm data and the theoretical equation was very important for the actual design and operation of the adsorption system. The most widely used equilibrium adsorption model was the Langmuir isotherm model, whose equation was as follows:

$$\frac{C_e}{q_e} = \frac{1}{K_e q_{max}} + \frac{C_e}{q_{max}} \tag{6}$$

Among them, C_e is the concentration of adsorbate in the solution at equilibrium (g L⁻¹), q_e is the equilibrium content of adsorbate (g g⁻¹), K_e is the Langmuir equilibrium constant (L g⁻¹), q_{max} is the adsorption mass (g g⁻¹) required to cover a single layer on the adsorbent. The adsorption equilibrium experiment of BC/PU foam composites on *n*-hexane was carried out in an aqueous solution at 30 °C and pH 7.0. Figure 8 shows the functional relationship between the *n*-hexane adsorption capacity (q_e) and the *n*-hexane concentration (C_e) in the aqueous solution at the experimental equilibrium of BC/PU foam composites. Compared with pure PU, the Langmuir isotherm model provided a good linear fit for the *n*-hexane adsorption isotherm of BC/PU foam composites, as shown in Fig. 8b. According to the slope and intercept of Fig. 8b, the q_{max} and K_e values were evaluated respectively, as shown in Table 4. The Langmuir isotherm model and the adsorption equilibrium experimental data of *n*-hexane on the BC/PU foam composites had a good correlation ($R^2 > 0.96$), indicating that the adsorption of *n*-hexane on the surface of

Table 4 Langmuir isotherm parameters for pure PU foam and BC/PU foam composites

Adsorbents	q_{max} (g g ⁻¹)	K_e (ml mg ⁻¹)	R^2
Pure PU	11.6	286	0.996
BC/PU-0.5	16.4	885	0.991
BC/PU-1	21.9	1153	0.894
BC/PU-5	23.9	2548	0.841
BC/PU-10	15.3	1102	0.882

the BC/PU foam composites was uniform and single-layer. In this study, the maximum OSs adsorption capacity of BC/PU-5 foam composites was about 23.9 g g^{-1} . It should be pointed out that the *n*-hexane adsorption capacity of BC/PU foam composites may be affected by many factors, such as BC content, foam structure, BC characteristics (particle size, surface acidic functional groups, etc.) and experimental conditions (Wang et al. 2018b). The negative value of ΔG^0 (-4.4 kJ mol^{-1} , 298 K) implied that the adsorption process of BC/PU-5 to OSs was energetically conducive to spontaneous occurrence.

3.7 DFT calculations

3.7.1 Parameters of dipole moment and frontier molecular orbital energy

The frontier molecular orbital energy (highest occupied molecular orbital energy (E_{HOMO}), lowest unoccupied molecular orbital energy (E_{LUMO})), Mulliken population analysis and dipole moment (m) were selected for DFT calculation, the corresponding molecular structure parameters were obtained, which could be used to find the relevant factors affecting the adsorption capacity and adsorption rate. The main parameters were shown in Table S8.

3.7.2 Relationship between E_{HOMO}/μ and adsorption effectiveness

According to Tables 3, 4 and S8, there was a relationship between E_{HOMO} and adsorption capacity calculated by pseudo-second-order kinetic model and Langmuir isotherm model (Q_e or Q_{max}) and the correlation coefficients (R^2) were over 0.975. The higher E_{HOMO} value of the seven OSs had the higher adsorption capacity on BC/PU-5. The quantitative relationship between E_{HOMO} and Q_e or Q_{max} could be expressed as: $y = 0.311 - 0.004/(1 + e^{(x - 3.876)/0.095})$ and $y = 0.405 - 0.006/(1 + e^{(x - 141.574)/1.229})$, respectively. Based on Tables 4 and S8, the E_{HOMO} had the similar correlation with the pseudo-second-order kinetic constant k_2 and the correlation coefficients (R^2) were over 0.983. The quantitative relationship between E_{HOMO} and k_2 could be expressed as: $y = 0.311 - 0.009/(1 + e^{(x - 1.69)/0.039})$. Therefore, the E_{HOMO} of the seven OSs had close correlation with their adsorption affinity on BC/PU-5 in Fig. 9a–c. For example, *n*-hexane had the highest E_{HOMO} , which led to its highest adsorption capacity and fastest adsorption rate, which was consistent with the experimental result. A reasonable explanation for this correlation was that the adsorption of OSs on BC/PU-5 could be caused by the EDA interaction. The highest occupied molecular orbital could be regarded as a nucleophile, which boasted the function of giving electrons (electron donor). The higher E_{HOMO} of OSs molecule

indicated the stronger abilities of donating electron, which led to the easier integration of OSs molecule with BC/PU-5.

Based on the values of μ of OSs in Table S8, Q_e , k_2 in Table 3 and Q_{max} in Table 4, the relationship between the μ and the Q_e , k_2 , Q_{max} was investigated in Fig. 9d–f, respectively. The respective relational expression of μ and Q_e , k_2 and Q_{max} was: $y = 1992.981 - 1986.236/(1 + e^{(x - 4.967)/0.323})$, $y = 0.198 \times e^{(x/0.983)} + 7.27$ and $y = 32.672 - 22.876/(1 + e^{(x - 208.923)/19.981})$, respectively. The correlation coefficients (R^2) were over 0.997. Obviously, the adsorption affinity of OSs was a positive correlation with μ . It is well known that the μ is related to the polarity and the OSs with higher μ had a stronger polarity. The polarity of BC/PU-5 increased due to the hydroxyl modification form BC, the OSs with higher polarity should have higher adsorption affinity on polar BC/PU-5. Therefore, the OSs with higher μ have stronger adsorption affinity for BC/PU-5.

3.8 Proposed adsorption mechanism of OSs on BC/PU-5

The adsorption isotherm results indicated that BC/PU-5 had a strong adsorption affinity for OSs, possibly due to the following interaction mode between BC/PU-5 and OSs: (i) electrostatic attraction and hydrogen bonding forces, which could be verified by the effect of pH on the adsorption efficiency of OSs; (ii) EDA interaction, the E_{HOMO} of OSs was positively correlated with their uptake affinity; (iii) the μ value of OSs was positively correlated with its adsorption affinity in the non-hydrophobic interaction. In addition, partial hydrophobicity of BC/PU-5 and hydrophobic groups in OSs may contribute to adsorption affinity. Therefore, the adsorption of OSs on BC/PU-5 was a multi-mechanism adsorption. The adsorption efficiency of BC/PU-5 for OSs may be mainly due to EDA interaction and non-hydrophobic interaction.

The adsorption energy of *n*-hexane molecules on BC/PU-5 was significantly higher than other OSs, which was consistent with previous adsorption results, and could be attributed to the rotatable chemical bonds and polarizability. Other OSs were polar substances and *n*-hexane was non-polar substances. The non-polar sites of BC/PU-5 could capture non-polar OSs. For non-polar molecules, the larger the polarizability α , the larger the solution-induced dipole moment. The dipole moment of *n*-hexane was larger than that of octane, and the C–H group on the surface was more easily captured by BC/PU-5. In addition, Table S6 shows the net charge transfer results under different adsorption systems. Mulliken's charge analysis showed that when the structure reached a steady state, the charge transfer between *n*-hexane and the surface of BC/PU-5 (about 2.7 eV) was much higher than that of other OSs adsorption systems,

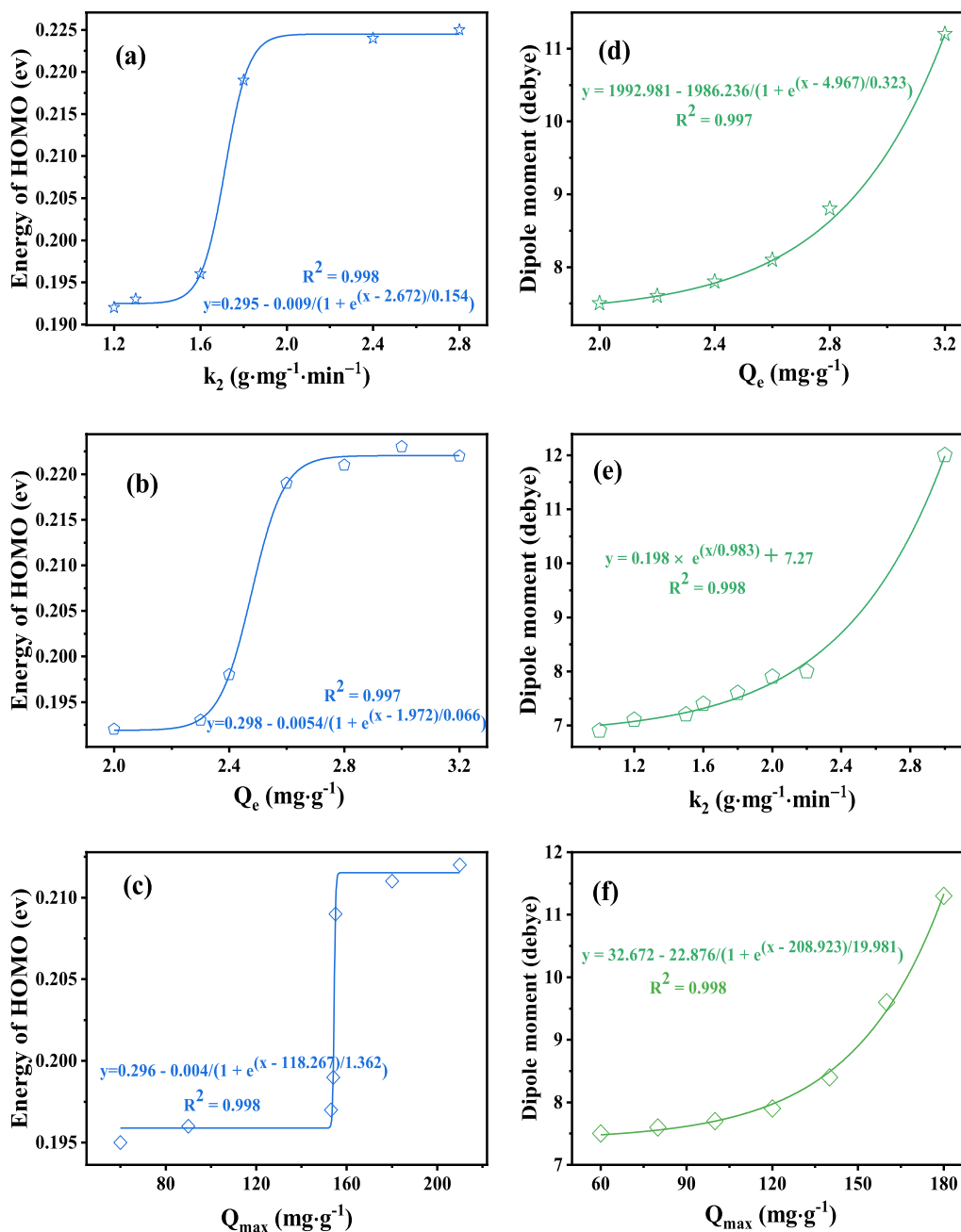


Fig. 9 The relationship between E_{HOMO} —adsorption affinity (a, b, c) and μ —adsorption affinity (d, e, f): calculated by pseudo—second—order kinetic model and Langmuir isotherm model

indicating that there was a strong interaction in the *n*-hexane-BC/PU-5 system (Fig. 10).

3.9 Reusability of BC/PU foam composites

In practical applications, the reusability of adsorbent materials was a relatively important property (Yuan et al. 2017; Zhao et al. 2021). In the above study, BC/PU-5 foam composites had the best adsorption performance, so the

reusability of BC/PU-5 foam composites was measured. The prepared BC/PU-5 foam composites were immersed in a sufficient amount of *n*-hexane, chlorobenzene and 1,2-dichloroethane, respectively. As shown in Fig. 11, it still maintained high adsorption performance in 5 cycles and could be reused many times without significant loss of adsorption performance. The results showed that the synthesized BC/PU-5 foam composites had good reutilization, which made it have good potential application value in organic solvent recovery.

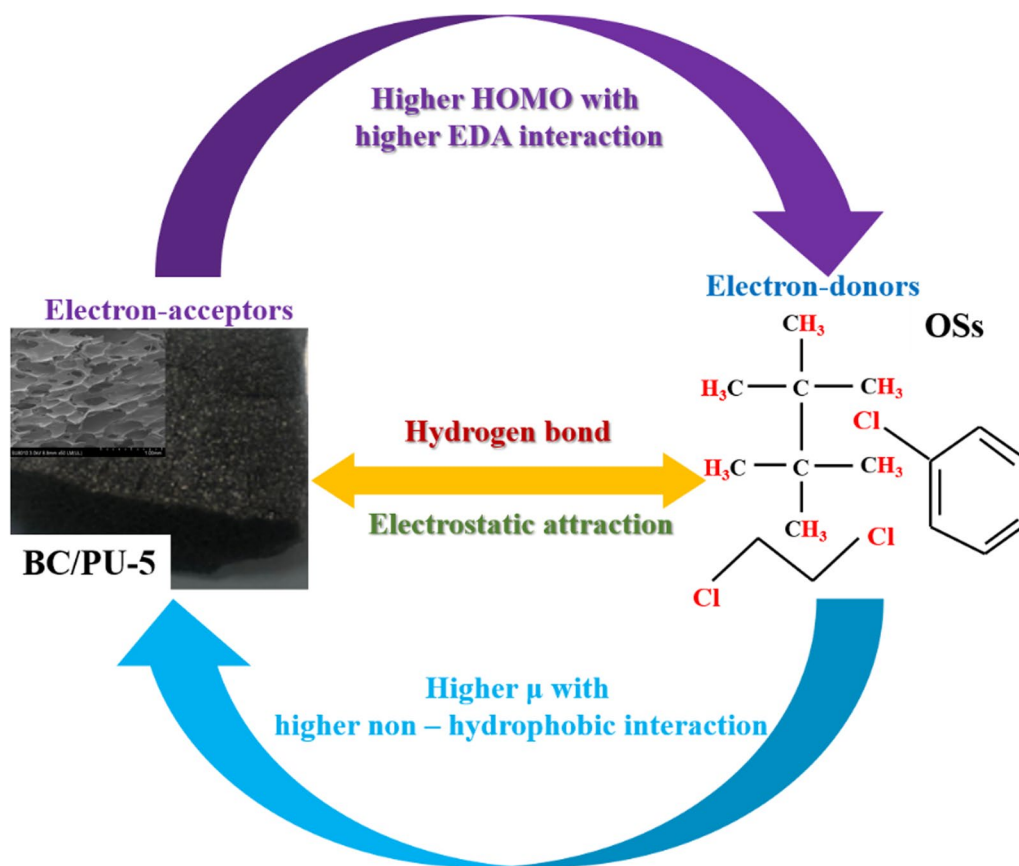


Fig. 10 Proposed adsorption mechanism of OSs on BC/PU-5

Finally, it can be confirmed with certainty that the prepared materials have an excellent combination of properties required for adsorbents suitable for practical applications. Relatively low cost, availability of reagents, and variety of preparation methods make BC/PU sponges ideal for applications in the field of wastewater treatment. More importantly, due to its good biocompatibility, its application in bioreactors as a filler is a further research goal in the future.

4 Conclusions

In summary, a new type of hydrophobic and oleophilic BC/PU-5 foam composite was prepared with BC powder as filler. It was revealed that BC powder effectively improved the adsorption efficiency of PU and the maximum adsorption capacity of BC/PU-5 was 23.6 g g^{-1} for *n*-hexane. The adsorption rate of OSs on BC/PU-5 was controlled by the chemisorption process, the adsorption kinetics and adsorption isotherms were fitted the pseudo-second-order kinetic model and Langmuir isotherm, respectively. The order of k_2 , Q_e and Q_{\max} of OSs was: octane < petroleum ether < soybean oil < chlorobenzene < 1,

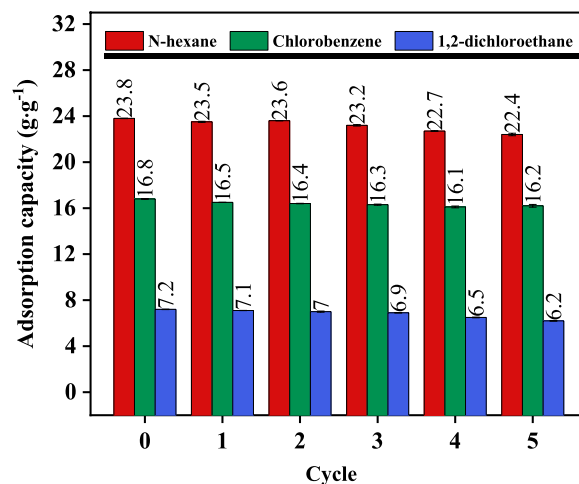


Fig. 11 OSs adsorption efficiency by BC/PU-5 foam composites for 5 cycles

2-dichloroethane < cyclohexane < *n*-hexane. The E_{HOMO} and μ of OSs calculated by DFT were highly correlated with absorption affinity (K_2 , Q_e and Q_{\max}). Hence, the contribution of OSs to the adsorption efficiency of BC/PU-5

may be mainly due to EDA interaction and non-hydrophobic interaction. Furthermore, the adsorption capacity did not change significantly after repeated recycling 5 times. Overall, the prepared BC/PU foam composites could be used as a potential candidate for separating OSs in engineering applications.

Supplementary Information The online version contains supplementary material available at <https://doi.org/10.1007/s42773-022-00153-2>.

Acknowledgements Not applicable.

Author contributions ZW: Conceptualization, Methodology, Writing—Original Draft; LH: Data curation, Investigation; MZ: DFT simulation; LD: Writing—Review & Editing; DH: Software, Validation; ST: Supervision; JC: Funding acquisition, Project administration. All authors read and approved the final manuscript.

Funding The project was supported by the National Primary Research & Development Plan (Grant No. 2018YFE0120300), the National Natural Science Foundation of China (Grant Nos. 42177115, 2191101496), Zhejiang Shuren University Scientific Research Start-up Funds (Grant No. 2020R011) and Zhejiang Provincial Education Department General Program (Grant No. Y202147579).

Availability of data and materials All data generated or analyzed during this study were included in this manuscript and its supplementary information files.

Declarations

Ethics approval and consent to participate All authors declare that there is no ethical violation in this manuscript. Also, this manuscript does not contain data belonging to others.

Competing interests The authors declare that they have no competing interests.

Open Access This article is licensed under a Creative Commons Attribution 4.0 International License, which permits use, sharing, adaptation, distribution and reproduction in any medium or format, as long as you give appropriate credit to the original author(s) and the source, provide a link to the Creative Commons licence, and indicate if changes were made. The images or other third party material in this article are included in the article's Creative Commons licence, unless indicated otherwise in a credit line to the material. If material is not included in the article's Creative Commons licence and your intended use is not permitted by statutory regulation or exceeds the permitted use, you will need to obtain permission directly from the copyright holder. To view a copy of this licence, visit <http://creativecommons.org/licenses/by/4.0/>.

References

- Alsweleh AM, Albahar HY, Alfawaz AM, Alsilme AS, Beagan AM, Alsahme AM, Almeataq MS, Alshahrani A, Alotaibi KM (2021) Evaluation of the adsorption efficiency of glycine-, iminodiacetic acid-, and amino propyl-functionalized silica nanoparticles for the removal of potentially toxic elements from contaminated water solution. *J Nanomater* 2021:6664252
- Akemoto Y, Sakti SCW, Kan M, Tanaka S (2021) Interpretation of the interaction between cesium ion and some clay minerals based on their structural features. *Environ Sci Pollut Res* 28(11):14121–14130
- Benally C, Messele SA, El-Din MG (2019) Adsorption of organic matter in oil sands process water (OSPW) by carbon xerogel. *Water Res* 154:402–411
- Brusseau ML (2019) The influence of molecular structure on the adsorption of PFAS to fluid-fluid interfaces: using QSPR to predict interfacial adsorption coefficients. *Water Res* 152:148–158
- Chang SH (2020) Utilization of green OSs in solvent extraction and liquid membrane for sustainable wastewater treatment and resource recovery—a review. *Environ Sci Pollut Res* 27(26):32371–32388
- Chen C, Zhu H, Li B-G, Zhu S (2021) Fabrication of metal-organic framework/polymer composites via a one-pot solvent crystal template strategy. *ACS Applied Polymer Materials* 3(4):2038–2044
- Chen MX, He FF, Hu DW, Bao CZ, Huang Q (2020) Broadened operating pH range for adsorption/reduction of aqueous Cr(VI) using biochar from directly treated jute (*Corchorus capsularis* L.) fibers by H3PO4. *Chem Eng J* 381:122739
- Gao X, Wu L, Xu Q, Tian W, Li Z, Kobayashi N (2018) Adsorption kinetics and mechanisms of copper ions on activated carbons derived from pinewood sawdust by fast H3PO4 activation. *Environ Sci Pollut Res* 25(8):7907–7915
- Ghafari M, Cui YB, Mali A, Atkinson JD (2019) Phenol adsorption and desorption with physically and chemically tailored porous polymers: mechanistic variability associated with hyper-cross-linking and amination. *J Hazard Mater* 361:162–168
- Goo S, Yook S, Park SY, Im W, Youn HJ (2019) Mechanical properties and soiling resistance of paper with polyurethane coating reinforced with cellulose nanomaterials. *BioResources* 14(4):8973–8986
- Guselnikova O, Barras A, Addad A, Sviridova E, Szunerits S, Postnikov P, Boukherroub R (2020) Magnetic polyurethane sponge for efficient oil adsorption and separation of oil from oil-in-water emulsions. *Sep Purif Technol* 240:116627
- Jia L, Yang J, Zhao W, Jing X (2019) Air-assisted ionic liquid dispersive liquid-liquid microextraction based on solidification of the aqueous phase for the determination of triazole fungicides in water samples by high-performance liquid chromatography. *RSC Adv* 9(63):36664–36669
- Khasri A, Ahmad MA (2018) Adsorption of basic and reactive dyes from aqueous solution onto Intsia bijuga sawdust-based activated carbon: batch and column study. *Environ Sci Pollut Res* 25(31):31508–31519
- Khosravi M, Azizian S (2015) Synthesis of a novel highly oleophilic and highly hydrophobic sponge for rapid oil spill cleanup. *ACS Appl Mater Interfaces* 7(45):25326–25333
- Kuo M-C, Shau S-M, Su J-M, Jeng R-J, Juang T-Y, Dai SA (2012) Preparation of supramolecular extenders with precise chain lengths via iterative synthesis and their applications in polyurethane elastomers. *Macromolecules* 45(13):5358–5370
- Li J, Xu C, Zhang Y, Wang R, Zha F, She H (2016) Robust superhydrophobic attapulgite coated polyurethane sponge for efficient immiscible oil/water mixture and emulsion separation. *J Mater Chem A* 4(40):15546–15553
- Li W, Mu B, Yang Y (2019a) Feasibility of industrial-scale treatment of dye wastewater via bio-adsorption technology. *Biores Technol* 277:157–170
- Li Z, Liu X, Huang Z, Hu S, Wang J, Qian Z, Feng J, Xian Q, Gong T (2019b) Occurrence and ecological risk assessment of disinfection byproducts from chlorination of wastewater effluents in East China. *Water Res* 157:247–257
- Lu P, Huang S, Shen Y, Zhou C, Shao L (2021) Mechanical performance analysis of polyurethane-modified asphalt using molecular dynamics method. *Polym Eng Sci* 61(9):2323–2338

- Lundin JG, McGann CL, Daniels GC, Streifel BC, Wynne JH (2017) Hemostatic kaolin-polyurethane foam composites for multifunctional wound dressing applications. *Mater Sci Eng, C* 79:702–709
- Luo G, Jin Z, Dong Y, Huang J, Zhang R, Wang J, Li M, Shen Q, Zhang L (2018) Preparation and performance enhancements of wear-resistant, transparent PU/SiO₂ superhydrophobic coating. *Surf Eng* 34(2):139–145
- Maddalena L, Carosio F, Gomez J, Saracco G, Fina A (2018) Layer-by-layer assembly of efficient flame retardant coatings based on high aspect ratio graphene oxide and chitosan capable of preventing ignition of PU foam. *Polym Degrad Stab* 152:1–9
- Meng F, Qiao Z, Yao Y, Luo J (2018) Synthesis of polyurethanes with pendant azide groups attached on the soft segments and the surface modification with mPEG by click chemistry for antifouling applications. *RSC Adv* 8(35):19642–19650
- Meng L, Li W, Bao M, Sun P (2019) Great correlation: Biodegradation and chemotactic adsorption of *Pseudomonas synxantha* LSH-7⁺ for oil contaminated seawater bioremediation. *Water Res* 153:160–168
- Mikusova I, Mikus P, Stodola J (2020) The effect of mechanical properties of a rubber compound on tyre wear. *Trans Famena* 44(3):73–80
- Moraes DS, Rodrigues EMS, Lamarao CN, Marques GT, Rente AFS (2019) New sodium activated vermiculite process. testing on Cu²⁺ removal from tailing dam waters. *J Hazard Mater* 366:34–38
- Morita Y, Koizumi G, Sakamoto H, Suye S-I (2017) Evaluation of protein adsorption onto a polyurethane nanofiber surface having different segment distributions. *Mater Chem Phys* 187:1–4
- Neimark AV, Grenev I (2020) Adsorption-induced deformation of microporous solids: a new insight from a century-old theory. *J Phys Chem C* 124(1):749–755
- Pan Y, Cai W, Du J, Song L, Hu Y, Zhao H (2020) Lanthanum phenylphosphonate-based multilayered coating for reducing flammability and smoke production of flexible polyurethane foam. *Polym Adv Technol* 31(6):1330–1339
- Piai L, Dykstra JE, Adishakti MG, Blokland M, Langenhoff AAM, van der Wal A (2019) Diffusion of hydrophilic organic micropollutants in granular activated carbon with different pore sizes. *Water Res* 162:518–527
- Pinto ERP, Barud HS, Silva RR, Palmieri M, Polito WL, Calil VL, Messaddeq Y (2015) Transparent composites prepared from bacterial cellulose and castor oil based polyurethane as substrates for flexible OLEDs. *J Mater Chem C* 3(44):11581–11588
- Sato T, England MW, Wang L, Urata C, Kakiuchida H, Hozumi A (2018) Polyurethane-based ionogels exhibiting durable thermoresponsive optical behavior under high-temperature conditions. *J Nanosci Nanotechnol* 18(1):195–201
- Simha P, Lalander C, Ramanathan A, Vijayalakshmi C, McConville JR, Vinneras B, Ganesapillai M (2018) What do consumers think about recycling human urine as fertiliser? Perceptions and attitudes of a university community in South India. *Water Res* 143:527–538
- Singh R, Singh B, Tarannum H (2019) Mechanical properties of jute fiber-reinforced UP/PU hybrid network composites. *Polym Polym Compos* 27(9):546–556
- Tahir H, Sultan M, Akhtar N, Hameed U, Abid T (2016) Application of natural and modified sugar cane bagasse for the removal of dye from aqueous solution. *J Saudi Chem Soc* 20:S115–S121
- Tandjaoui N, Abouseoud M, Couvert A, Amrane A, Tassiss A (2019) A combination of absorption and enzymatic biodegradation: phenol elimination from aqueous and organic phase. *Environ Technol* 40(5):625–632
- Vandamme D, Gheysen L, Muylaert K, Foubert I (2018) Impact of harvesting method on total lipid content and extraction efficiency for *Phaeodactylum tricornutum*. *Sep Purif Technol* 194:362–367
- Wang C, Huang R, Sun R (2020) Green one-spot synthesis of hydrochar supported zero-valent iron for heterogeneous Fenton-like discoloration of dyes at neutral pH. *J Mol Liq* 320:114421
- Wang C, Sun R, Huang R (2021) Highly dispersed iron-doped biochar derived from sawdust for Fenton-like degradation of toxic dyes. *J Clean Prod* 297:126681
- Wang C, Wang H (2018) Carboxyl functionalized *Cinnamomum camphora* for removal of heavy metals from synthetic wastewater-contribution to sustainability in agroforestry. *J Clean Prod* 184:921–928
- Wang C, Wang H, Gu G (2018a) Ultrasound-assisted xanthation of cellulose from lignocellulosic biomass optimized by response surface methodology for Pb (II) sorption. *Carbohydr Polym* 182:21–28
- Wang N, Wu R, Fu Q, Wang H, Zhang Z, Ze H, Li X, Lian X, An Y (2018b) Immobilization of beta-Glucosidase BglC on decanedioic acid-modified magnetic nanoparticles. *Chem Eng Technol* 41(10):1949–1955
- Wu M-N, Maity JP, Bundschuh J, Li C-F, Lee C-R, Hsu C-M, Lee W-C, Huang C-H, Chen C-Y (2017) Green technological approach to synthesis hydrophobic stable crystalline calcite particles with one-pot synthesis for oil-water separation during oil spill cleanup. *Water Res* 123:332–344
- Xiang Y, Pang Y, Jiang X, Huang J, Xi F, Liu J (2018) One-step fabrication of novel superhydrophobic and superoleophilic sponge with outstanding absorbency and flame-retardancy for the selective removal of oily organic solvent from water. *Appl Surf Sci* 428:338–347
- Xu N, Wang X, Wang L, Zheng Y, Zhang F, Guo P (2019) Modification of PA/PU superfine non-woven fiber for “breath” property using collagen and vegetable tannins. *J Ind Text* 48(10):1593–1615
- Yuan D, Zhang T, Guo Q, Qiu F, Yang D, Ou Z (2017) A novel hierarchical hollow SiO₂@MnO₂ cubes reinforced elastic polyurethane foam for the highly efficient removal of oil from water. *Chem Eng J* 327:539–547
- Zhang Y, Lebedev M, Al-Yaseri A, Yu H, Xu X, Sarmadivaleh M, Barifcani A, Iglauer S (2018) Nanoscale rock mechanical property changes in heterogeneous coal after water adsorption. *Fuel* 218:23–32
- Zhao DL, Chung T-S (2018) Applications of carbon quantum dots (CQDs) in membrane technologies: a review. *Water Res* 147:43–49
- Zhao J, Xu L, Su Y, Yu H, Liu H, Qian S, Zheng W, Zhao Y (2021) Zr-MOFs loaded on polyurethane foam by polydopamine for enhanced dye adsorption. *J Environ Sci* 101:177–188